Secondary nontwist phenomena in area-preserving maps

C. Vieira Abud and I. L. Caldas

Citation: Chaos: An Interdisciplinary Journal of Nonlinear Science **22**, 033142 (2012); doi: 10.1063/1.4750040
View online: http://dx.doi.org/10.1063/1.4750040
View Table of Contents: http://scitation.aip.org/content/aip/journal/chaos/22/3?ver=pdfcov
Published by the AIP Publishing

Secondary nontwist phenomena in area-preserving maps

C. Vieira Abud[a] and I. L. Caldas[b]
Instituto de Física, Universidade de São Paulo, São Paulo, 05315-970 São Paulo, Brazil

(Received 17 January 2012; accepted 21 August 2012; published online 10 September 2012)

Phenomena as reconnection scenarios, periodic-orbit collisions, and primary shearless tori have been recognized as features of nontwist maps. Recently, these phenomena and secondary shearless tori were analytically predicted for generic maps in the neighborhood of the tripling bifurcation of an elliptic fixed point. In this paper, we apply a numerical procedure to find internal rotation number profiles that highlight the creation of periodic orbits within islands of stability by a saddle-center bifurcation that emerges out a secondary shearless torus. In addition to the analytical predictions, our numerical procedure applied to the twist and nontwist standard maps reveals that the atypical secondary shearless torus occurs not only near a tripling bifurcation of the fixed point but also near a quadrupling bifurcation. © *2012 American Institute of Physics*.
[http://dx.doi.org/10.1063/1.4750040]

Many Hamiltonian systems can basically be discretized by two-dimensional area-preserving maps. We can distinguish the many differences between maps by the so-called twist condition (or torsion); i.e., a condition that asserts the nondegeneracy of the frequencies. Twist and nontwist maps have been introduced for several dynamical systems. The compositions of their phase spaces have some similarity, but also special differences. One of the differences, and maybe the most relevant, is the existence of a torus without twist, sometimes called shearless torus, in nontwist maps. The scientific community has always considered that these shearless tori were characteristic of nontwist maps, but recent studies have shown they can also be found in twist maps. In this paper, we present a numerical investigation identifying the onset of shearless tori around elliptic fixed points of standard nontwist and twist maps.

I. INTRODUCTION

The idea that Hamiltonian systems of two degrees of freedom can be represented by area-preserving maps of planar regions was first introduced by Henri Poincaré. One of the main advantages of these maps is that they are efficient from a computational point of view. Owing to their high performance, area-preserving maps have received much attention in both theoretical[1–3] and experimental[4,5] investigations.

Nowadays, it is well accepted that the *universal* behavior of Hamiltonian systems can be synthesized by area-preserving maps. Nevertheless, this universal behavior depends on a condition that asserts the nondegeneracy of the frequencies in the integrable regime, the so-called twist condition. (The mathematical definition of the twist condition will be given in Sec. II.) For example, the twist condition is defined for area-preserving maps so that if a map possesses orbits with frequencies (rotation numbers) that increase monotonically, then the map satisfies the twist condition and it is called a twist map; otherwise, we have a nontwist map. The twist condition is assumed in several mathematical theorems such as the Poincaré-Birkhoff theorem, Aubry-Matter theorem, and the well-known Kolmogorov-Arnold-Moser (KAM) theorem, which in the second half of the 20th century pointed out the persistence of quasi-periodic motion under small perturbations. These theorems are the basis of twist map scenario but they not been verified in the nontwist case, and there may be different features in the phase space.

Hence, from a topological point of view, the phase spaces of twist and nontwist maps have some differences. In particular, it had been expected that some atypical phenomena such as the presence of an invariant torus without twist, and the separatrix reconnection process were only observed in nontwist maps. Nevertheless, Dullin *et al.* studied the resonant normal form around the neighborhood of elliptic fixed points of area-preserving maps and showed that shearless tori can emerge through an atypical bifurcation.[6] This shearless torus can eventually collide with a saddle-center bifurcation creating period-three orbits. Since the saddle-center bifurcation is generic, the shearless tori are also generic[7] and we expect to find these tori in both nontwist and twist maps.

However, the application of the normal forms to identify shearless tori may be difficult for some maps, e.g., those introduced to describe nearly integrable systems in fluids and plasmas.[8,9] Thus, it is useful to introduce a numerical procedure to identify shearless tori around elliptic fixed points. In the present paper, we introduce a simple numerical procedure, based on the variation of the rotation number profile with the control parameter, in order to identify the onset of secondary shearless tori, i.e., a shearless tori that appear within islands of stability, and illustrate not only the concomitant creation of period-three orbits but also a new unpredicted period-four orbits. As examples, we apply this procedure to the nontwist and twist standard maps.

The paper is organized as follows. Section II presents formulas that are used throughout the paper. Section III

[a]Author to whom correspondence should be addressed. Electronic mail: cabud@if.usp.br.
[b]ibere@if.usp.br.

reviews some properties of standard nontwist maps (SNMs) and investigates a tripling bifurcation identified by a secondary shearless torus inside an island. Our main goal is achieved in Sec. IV, where we show that the secondary shearless torus may also exist in the standard twist map (SM) near of the tripling and quadrupling bifurcation of an elliptic fixed point. Furthermore, we present a reconnection process for the first time for the standard map. Conclusions are given in Sec. V.

II. AREA PRESERVATION AND THE TWIST CONDITION

Generally, two dimension Hamiltonian systems can be described by area-preserving maps having the form

$$J_{n+1} = J_n + f(\theta_n), \tag{1}$$

$$\theta_{n+1} = \theta_n - g(J_{n+1}), \tag{2}$$

where $J \in \Re$ and $\theta \in [-\pi; \pi]$ are action-angle variables whereas $f(\theta_n)$ is a 2π-periodic function. In most studies, the function $g(J)$ is monotonic. However, one finds situations where $g(J)$ has an extremum (i.e., $g'(J) = 0$), resulting in a degeneracy in the frequency. Both cases can be checked by the so-called twist condition

$$\left|\frac{\partial\theta_{n+1}(J_n, \theta_n)}{\partial J_n}\right| = |g'(J_{n+1})| \geq c > 0, \tag{3}$$

where c is a real number. If Eq. (3) is fulfilled, then the map is called *twist* and $g(J)$ is monotonic. On the other hand, if a map violates the twist condition, it is called *nontwist* and it has a nonmonotonic function $g(J)$.

An important quantity to verify the monotonicity of orbits is the rotation number. In general, the rotation number, ω, of an orbit is defined by

$$\omega = \lim_{n\to\infty} \frac{1}{n} \sum_{n=1}^{\infty} (x_{n+1} - x_n). \tag{4}$$

From Eq. (4), we see that the rotation number exists when a well-defined limit exists. In this case, the x-coordinate (abscissa coordinate) is lifted to the entire real line; i.e., x_n is not modulated. Hence, it is referred to as the global rotation number. If, the initial point returns to the same point after n-iterations, then one has a periodic orbit with rational rotation number m/n, where n is the period and m is the integer number of times that the orbit passed through the x-domain. On the other hand, quasi-periodic orbits (tori) are represented by an irrational rotation number, whereas for chaotic orbits the sum in Eq. (4) does not converge.

In this paper, we are interested in localized regions of the phase space to identify secondary shearless tori and observe their parameter dependence through an island of stability. Hence, we introduce the internal rotation number. Similar to the case of using the global rotation number to show (monotonic or nonmonotonic) profiles of invariant curves that cross the entire phase space, the internal rotation number allows us to measure the torsion of each torus within one regular island. Since the internal rotation number is a measure of the rotation of a torus with respect to the elliptic fixed point of an island, it is defined as

$$\omega_{in} = \lim_{n\to\infty} \frac{1}{2\pi n} \sum_{n=1}^{\infty} P_n(x, y)\hat{\theta}P_{n+1}(x, y), \tag{5}$$

where $P_n\hat{\theta}P_{n+1}$ means the angle θ between two consecutive points and (x, y) are the coordinates of the two-dimensional map. The angle θ is normalized by 2π so that the values returned belong to the range [0,1]. Note that the internal rotation number does not have a lifted coordinate. However, proceeding in this way, a rational internal rotation number (m/n) describes a periodic orbit while an irrational number represents a quasi-periodic orbit. For a chaotic orbit, Eq. (5) does not converge, likewise the global rotation (Eq. (4)). For our purposes, the main use of the internal rotation number is to measure the rotation of the torus within just one island that, for example, belongs to a chain of islands. Hence, the results discussed in this paper relate to local properties and not global properties as is usually done.

III. NONTWIST GLOBAL PHENOMENA

This section considers the SNM. The map can be obtained by choosing a nonmonotonic function for $g(J)$ in Eq. (2). Since $g(J)$ is nonmonotonic, it may have a countable number of extrema (J_S). The Taylor series expansion of $g(J)$ around the extrema J_S gives

$$g(J) \approx g(J_S) + \frac{1}{2} g''(J_S)(J - J_S)^2. \tag{6}$$

Without loss of generality, since $g(J_S)$ is a constant, we choose $g(J_S) = 0$. Now, we introduce normalized variables: $x = \theta/2\pi$ and $y = J/J_S$. Finally, defining $a = \frac{1}{4\pi} g''(J_S)$ and $f(\theta) = -bJ_S \sin(\theta)$, Eqs. (1) and (2) become the SNM

$$X_{n+1} = X_n + a(1 - Y_{n+1}^2), \qquad mod 1 \tag{7}$$

$$Y_{n+1} = Y_n - b\, sin(2\pi X_n), \tag{8}$$

with $y \in \Re$. Usually, we limit the investigation to the range $a = [0; 1]$ and $b \in \Re$. The SNM is an area-preserving map that violates the twist condition; i.e., $\partial X_{n+1}/\partial Y_n = 0$ for $Y_n = b\sin(2\pi X_n)$.

Nontwist maps have received much attention from physicists and mathematicians. Many physical systems are modeled by nontwist maps, and they are of particular interest for continuous systems; e.g., the magnetic field lines in reversed shear tokamaks[10–13] and the zonal flows in geophysical fluid dynamics.[8] One important mathematical point is that many theorems (as the KAM theorem[14]) formulated for near-integrable Hamiltonian systems are not valid for nontwist systems since they assume the nondegeneracy of the frequencies.

Some properties of the nontwist map have been previously studied.[15–19] Owing to the violation of the twist condition, several nontwist phenomena are observed. All nontwist phenomena appear around the so-called *shearless curve*; i.e.,

a robust torus with maximum or minimum frequency. In the vicinity of the shearless torus emerge two adjacent sets of periodic orbits (chains of islands) of period p. According to the period p of the island chains, the island positions on each side of the shearless curve in the phase space may change. Thus, if the orbits have even p, then the orbits on each side have the same stability; i.e., if one is a center (saddle) there is also a center (saddle) on the other side. Otherwise, if p is odd, the stability type differs.

As the perturbation parameter increases, the two island chains approach each other and reconnect[15,19] such that the periodic points do not change their type. After the reconnection process, the two island chains are separated by invariant curves, called meanders, with a nonmonotonic rotation number profile containing a shearless curve. Figure 1 shows the typical phase space of SNM. From Fig. 1, for $b=0.5232$ and $a=0.3640$, we see two chains of $\frac{1}{3}$ islands separated by nontwist invariant tori, the meanders. This separation of the $\frac{1}{3}$ chains of islands means that reconnection process has previously occurred. The inset of Fig. 1 shows the profile of the global rotation number. The mentioned rotation number is obtained by choosing 400 different initial conditions along the line $X=0$ and iterating 10^6 times. Note that when the profile is around the meanders, the typical curve is a kind of *bump* with maximum rotation. This maximum is due to the shearless torus (red line in the phase space). The profile saturates when it enters the $\frac{1}{3}$ island, and we have the rotation $\omega_{global}=\frac{1}{3}$.

In Fig. 2, we choose $b=0.800$ and $a=0.455$ to observe the mixing of chaos and small islands in the Poincaré section. At this point, the meandering curves are almost wiped out and, the shearless torus is the last invariant torus to be destroyed (see the inset of the magnified phase space). For some parameter combinations, the meandering curves are destroyed and the two chaotic regions are unified.[17,20] Then, the orbits in SNM develop a transport in the Y-coordinate, being affected only by the stickiness effect of the remnant islands.[21]

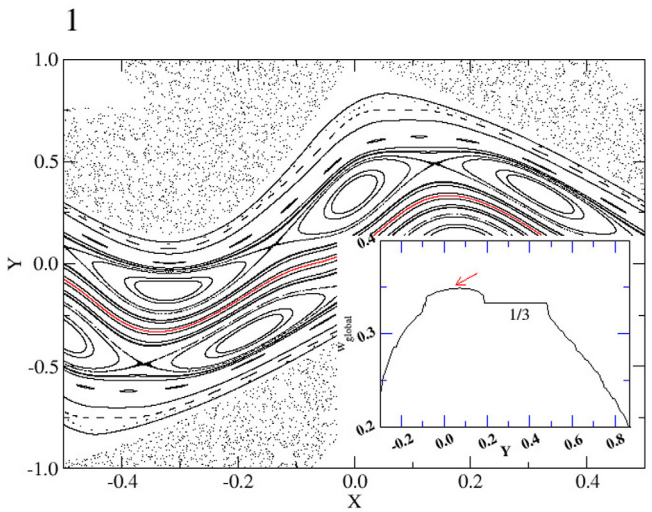

FIG. 1. Phase space for the nontwist map with $b=0.5232$ and $a=0.3640$. The inset shows the global rotation number (Eq. (4)) for a line of initial conditions on the line $X=0$. The shearless torus is indicated by an arrow in the inner box and corresponds to the red line in the phase space.

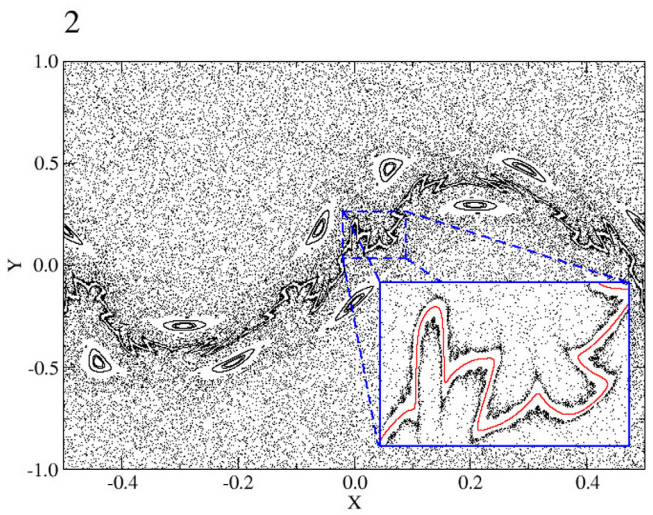

FIG. 2. Phase space for the nontwist map with $b=0.800$ and $a=0.455$. The blue square inside the figure is a magnification emphasizing the surviving shearless torus.

Most studies on maps focus on the global properties of the phase space. In this paper, we investigate the secondary resonances of a system to check more precisely topological properties that may have been missed in previous global investigations.

A. S-shearless torus (tripling bifurcation)

Several articles have reported primary shearless tori, like those shown in Figs. 1 and 2. Included in this list are: nontwist Hamiltonian systems[15,17,20] and even non-Hamiltonian systems.[22]

In this section, we explore the possibility of finding a torus without twist near an elliptic fixed point of islands. We refer to such tori as secondary shearless (s-shearless) tori owing to the topological similarity to the global shearless structure.

In Fig. 3, we have four phase spaces showing the evolution of only one island that belongs to a period-two chain. For the phase spaces of Fig. 3, we fix $b=0.8$ and change a in the range $a\in[0.5430;0.5517]$. On the right side of each phase space, we show the internal rotation number profile, calculated choosing 400 initial conditions along the line $X=0$ within the island. From Fig. 3(a) with $a=0.543$, we observe that the tori within the islands are disposed following the geometry of the islands and that the internal rotation profile is monotonic; i.e., each rotation number is related to a single torus. We emphasize that the top of the *bump* in the profile of the rotation indicates the position of the elliptic fixed point. In fact, according to the definition of Eq. (5), the elliptical point has an internal rotation number equal to unity, but we need to avoid the exact elliptic point in order to plot a smooth curve. The blue dashed line was introduced in each picture to assist in identifying the fixed point. The left and right sides of the blue dashed line relate to the orbits above and below the elliptic fixed point, respectively. Therefore, in the considered range for Y, the curve of internal rotation number is symmetrical for left and right sides.

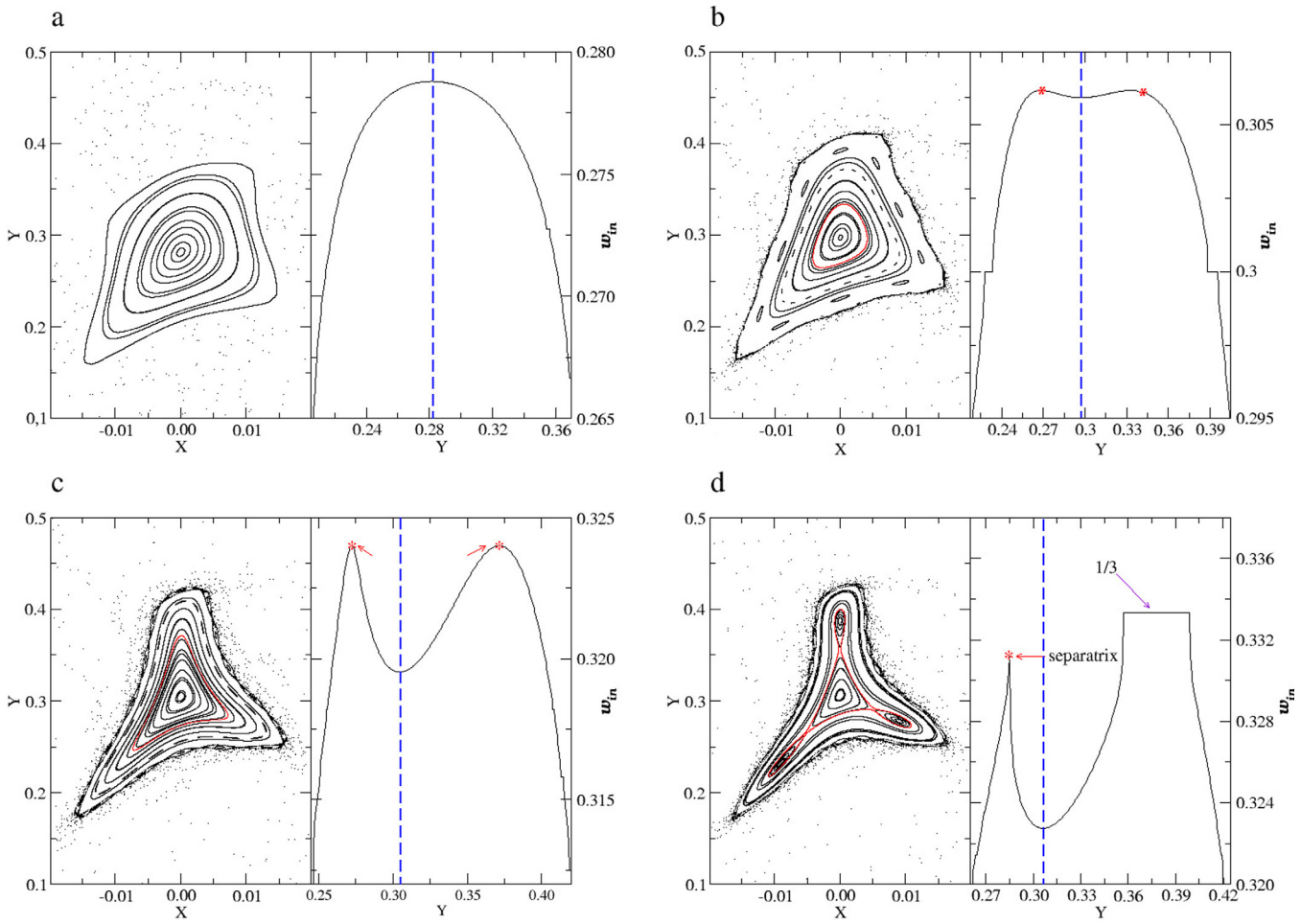

FIG. 3. Islands of stability for the nontwist map (left) with their related internal rotation number (right). In all cases, we fixed b = 0.8 and we chose one of the islands that belong to a period 2 chain of the phase space. In (a), we have $a = 0.543$ and the internal rotation number presents a monotonic profile. Figures (b) with $a = 0.5485$ and (c) with $a = 0.551$, show the emergency of a shearless torus. In the figure (d) with $a = 0.5517$, we see the creation of a period-three orbits inside the island.

In Fig. 3(b), we slightly modify the parameter a ($a = 0.5485$) and the internal rotation number shows the rise of a new *bump* above the elliptic fixed point, which is now a minimum point in a valley. The new profile of the internal rotation is nonmonotonic because we have the same rotation numbers related to more than one torus. In addition, the top of the *bump* relates to a torus with a zero derivative. The evolution of the s-shearless torus can be checked from following plots of Fig. 3. Note that in Fig. 3(c), the *bump* increases to rotation numbers higher than those in Fig. 3(b) and the internal invariant circles are deformed, indicating the start of a saddle-center bifurcation. Finally, in Fig. 3(d), we have the emergence of tripling bifurcation. Owing to our line of initial conditions, the left *bump* corresponds to the separatrix and the right *bump* to the $\frac{1}{3}$ bifurcation. After the tripling bifurcation, the s-shearless torus no longer exists and the separatrix of the period-three orbit continues to the outside to become a cantorus.

Our results are in agreement with Ref. 6, where the authors pointed out that a tripling bifurcation of the elliptic fixed point is always due to a saddle-center bifurcation of a shearless torus. In that paper, the authors used the resonant normal form for area-preserving maps in the neighborhood of an elliptic fixed point, finding the emergence of a shearless torus through mathematical arguments. Our approach is quite different and we introduce a tool—the internal rotation number—that allows us to verify the evolution of the shearless torus onset and the topology. The reader may think that it is an expected phenomenon since we are studying nontwist phenomena in a nontwist map. We emphasize that this has never been shown before for nontwist maps. Moreover, since a saddle-center bifurcation is generic, we expect to see the same event even for twist maps. In the next section, we present the emergence of an s-shearless torus in the standard map for a similar case of tripling bifurcation and a new scenario, a quadrupling bifurcation.

IV. STANDARD MAP

Before showing the shearless torus in standard map, we introduce some basic properties of the map. The SM, also called the Chirikov-Taylor map,[23] can be obtained using the relations: $f(\theta) = K \sin\theta$ and $g(J) = J$ in Eqs. (1) and (2), respectively. Thus, the map becomes

$$J_{n+1} = J_n + \frac{K}{2\pi}\sin(2\pi\theta_n), \qquad mod 1 \tag{9}$$

$$\theta_{n+1} = \theta_n - J_{n+1}, \qquad mod 1, \tag{10}$$

where $K \geq 0$ is the nonlinearity parameter. The SM is an area-preserving map that meets the twist condition; i.e., $\partial\theta_{n+1}/\partial J_n \neq 0$. For $K = 0$, the map is integrable and only periodic and quasi-periodic orbits are possible. The chaotic dynamics are achieved by increasing the parameter K, with appropriate initial conditions.

Unlike the case for the SNM, the formation of the invariant tori in the SM is predicted by KAM theory, and the destruction of tori and the generation of islands are also well predicted by the Poincaré-Birkhoff theorem. The SM models several physical systems: e.g., the cyclotron particle accelerator[24] and the Frenkel-Kontorova model of condensed matter physics.[25] There are also applications in plasma physics,[9] celestial dynamics,[26] and even quantum mechanics.[27]

In this example, we study the SM of high-perturbation regime. The phase space consists of two visible regular islands immersed in a chaotic sea. Hence, to obtain the internal rotation number, we follow the evolution of one of two main islands. For $K = 4$, these islands emerge from a split of a major island around the stable periodic orbit ($\theta = 0.5$ and $J = 0$). Therefore, the islands have suffered several bifurcations and have reduced size because the system possesses stronger perturbation and the chaos tends to spread.

A. S-shearless torus (tripling bifurcation)

Figure 4 shows the evolution of one of the islands, starting from $K = 5.35$. The phase space is seen to have symmetry across the diagonal ($J = 2\theta$, dashed curve in Fig. 4(a)), which we use for the initial conditions of the internal rotation number, as done in Sec. II A for SNM. The profile of the internal rotation number is a monotonic curve, characteristic of twist regions. Increasing the parameter to $K = 5.50$ is sufficient for the formation of bumps as shown in Fig. 4(b). The presence of a minimum point in the rotation profile indicates a torus without twist. This shearless torus is not expected in the theory of twist maps and means that the twist condition is not applicable, locally, in some regions of the phase space.

In Figure 4(c), we verify that the bumps approach $\omega_{in} = 1/3$ and all tori have decreasing the internal rotational number, driven by the bumps. The phase space of Fig. 4(c) with $K = 5.554$ shows clearly the emergency of a saddle-center bifurcation. When the internal rotation number reaches the rational value of 1/3, there is a tripling bifurcation inside the main island as shown in Fig. 4(d) with $K = 5.56$.

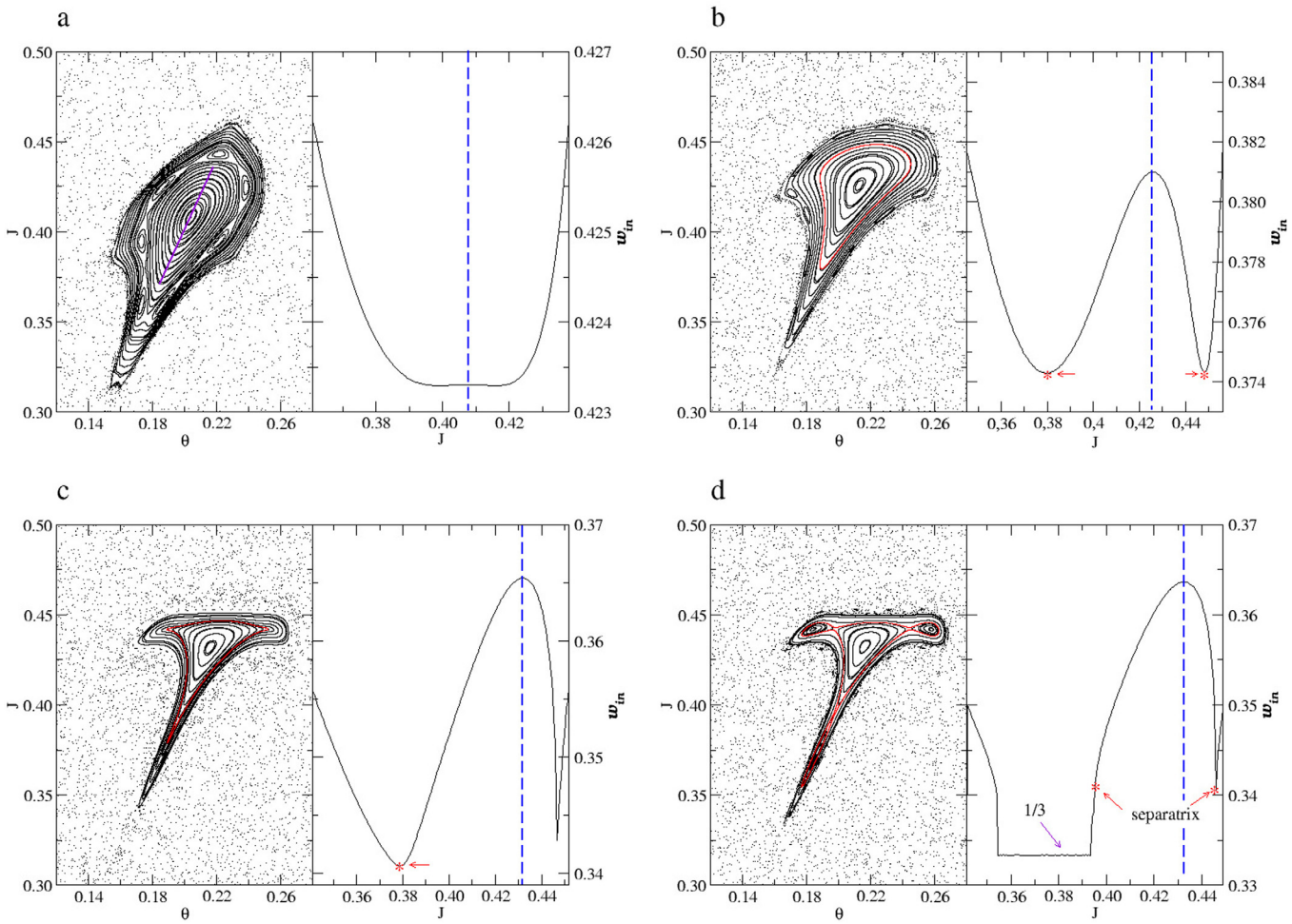

FIG. 4. Islands of stability for the standard twist map (left) with their related internal rotation number (right). In (a), we have $K = 5.35$ and the internal rotation number presents a monotonic profile. Figure (b) with $K = 5.50$ and (c) with $K = 5.554$, show the presence of a shearless torus. In figure (d) with $K = 5.56$, we see the creation of a period-3 orbit inside the island.

In the range where the s-shearless torus exists, there may be many rational internal rotation numbers. If the number is a lowest-order rational number in the considered range, there should be visible nontwist bifurcations. In Subsection IV B, we describe these bifurcations in terms of their phase space.

B. Reconnection process of the s-shearless torus

In the interval where the s-shearless torus exists, the internal rotation number may be a rational value. For example, between Figs. 4(a) and 4(b), the rotation number of the s-shearless torus, identified for the SM, passed the rational value 0.4. This value is the most prominent because it is the lowest-order rational in the interval considered. Hence, near this value, there should be nontwist bifurcations. From Fig. 5(a) ($K = 5.428313$), we see that before approximately $\omega_{in} = 0.4$, there is a small range in the phase space where the s-shearless torus causes a new torsion. When $K = 5.428320$ (Fig. 5(b)), there is a saddle-center $\frac{4}{10}$ bifurcation. Afterward, a new saddle-center $\frac{4}{10}$ bifurcation emerges. Therefore, in Fig. 5(c) with $K = 5.428330$, we have four $\frac{4}{10}$ periodic orbits, two being stable (elliptic) and two being unstable (hyperbolic). We should clarify that the phase space shows 10-periodic orbits that form a chain of islands after four turns around the elliptic fixed point, therefore, this explains why the rotation number is $\frac{4}{10}$ instead of not simply $\frac{2}{5}$.

Suddenly, at $K = 5.428340$, the stable and unstable manifolds of the two unstable (hyperbolic) $\frac{4}{10}$ orbit undergo reconnection as shown in Fig. 5(d). Finally, Figs. 5(e) and 5(f) with $K = 5.428343$ and $K = 5.428352$, respectively, show decoupling of the chains.

This is a typical scenario of nontwist maps creating invariant tori that do not follow the KAM theorem. In particular, the scenario described by Fig. 5 is identical to the odd-period reconnection sequence of the standard nontwist map, whose rotation number profile is characterized by the onset of two *outer* shearless tori in addition to the previous one.[15] It means that in Fig. 5(a), in addition to the main bump verified in Fig. 4, other two outer shearless exist to generate the two $\frac{4}{10}$ chain of islands.

As stated previously, this kind of bifurcation has been extensively studied for nontwist maps. However, we are dealing with a twist map whose global properties follow the KAM theorem. It does not mean that we need to re-evaluate the theory for twist maps but, at least locally for some range of phase space, there is the possibility to break down some behaviors.

We should call attention to the similarity between Fig. 5 of the present paper and Fig. 7 of Dullin *et al.* in Ref. 6 for the Hénon map. Both systems are twist maps, but the equations are quite different. This reveals the generality of the bifurcations that appears in the presence of an s-shearless torus within a stable island.

C. S-shearless torus (quadrupling bifurcation)

Besides the case that leads to the tripling bifurcations, we also find a new emergency of s-shearless tori that bifurcate in four islands (see Figs. 6(a)–6(c)) This case occurs before the triplication of the elliptic fixed point and represents a novelty faced with the analytical predictions.[6]

Thus, for $K = 5.074$, Fig. 6(c) shows four islands containing two independent $\frac{1}{2}$ stable periodic orbits. To illustrate this bifurcation, in Fig. 6(d), we present internal rotation

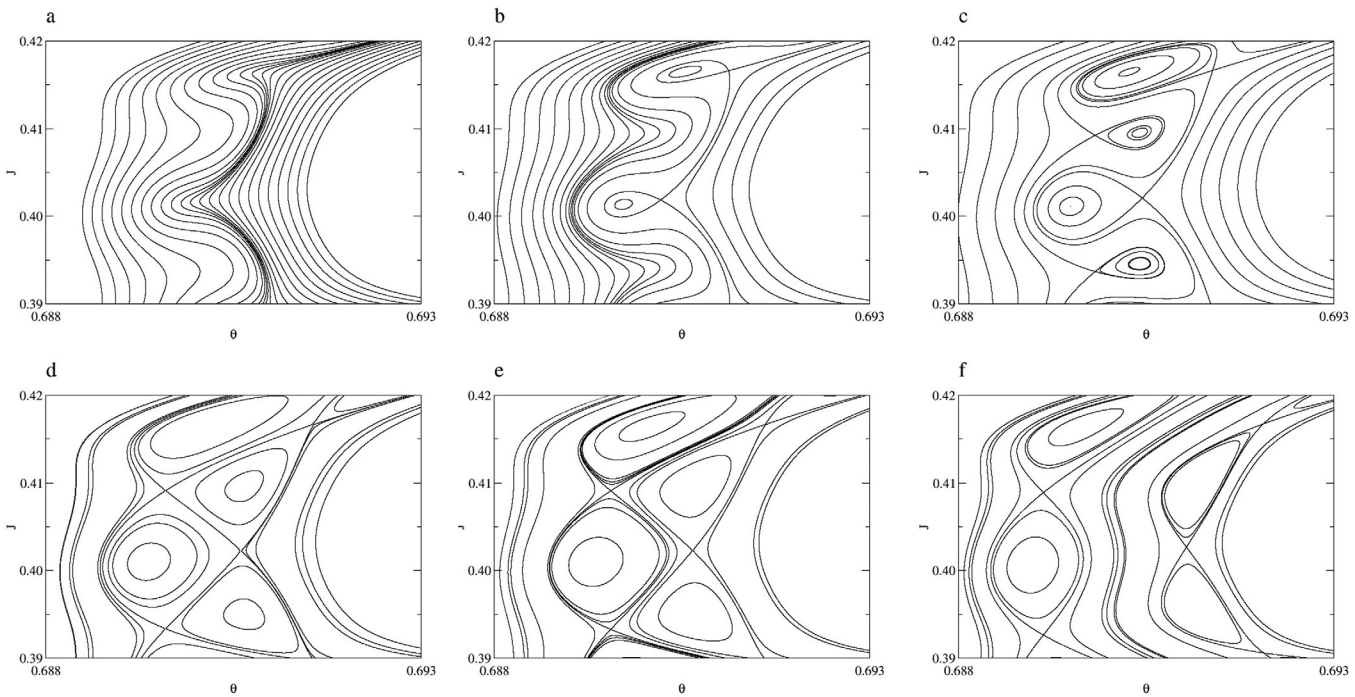

FIG. 5. Reconnection process of the shearless torus near an elliptic fixed point of the standard map. The sequence of bifurcations is: (a) torsion, $K = 5.428313$; (b) saddle-center $\frac{4}{10}$, $K = 5.428320$; (c) a new saddle center $\frac{4}{10}$, $K = 5.428330$; (d) reconnection process, $K = 5.428340$; (e) $K = 5.428343$; and (f) $K = 5.428352$ show the decoupling in two chain of islands.

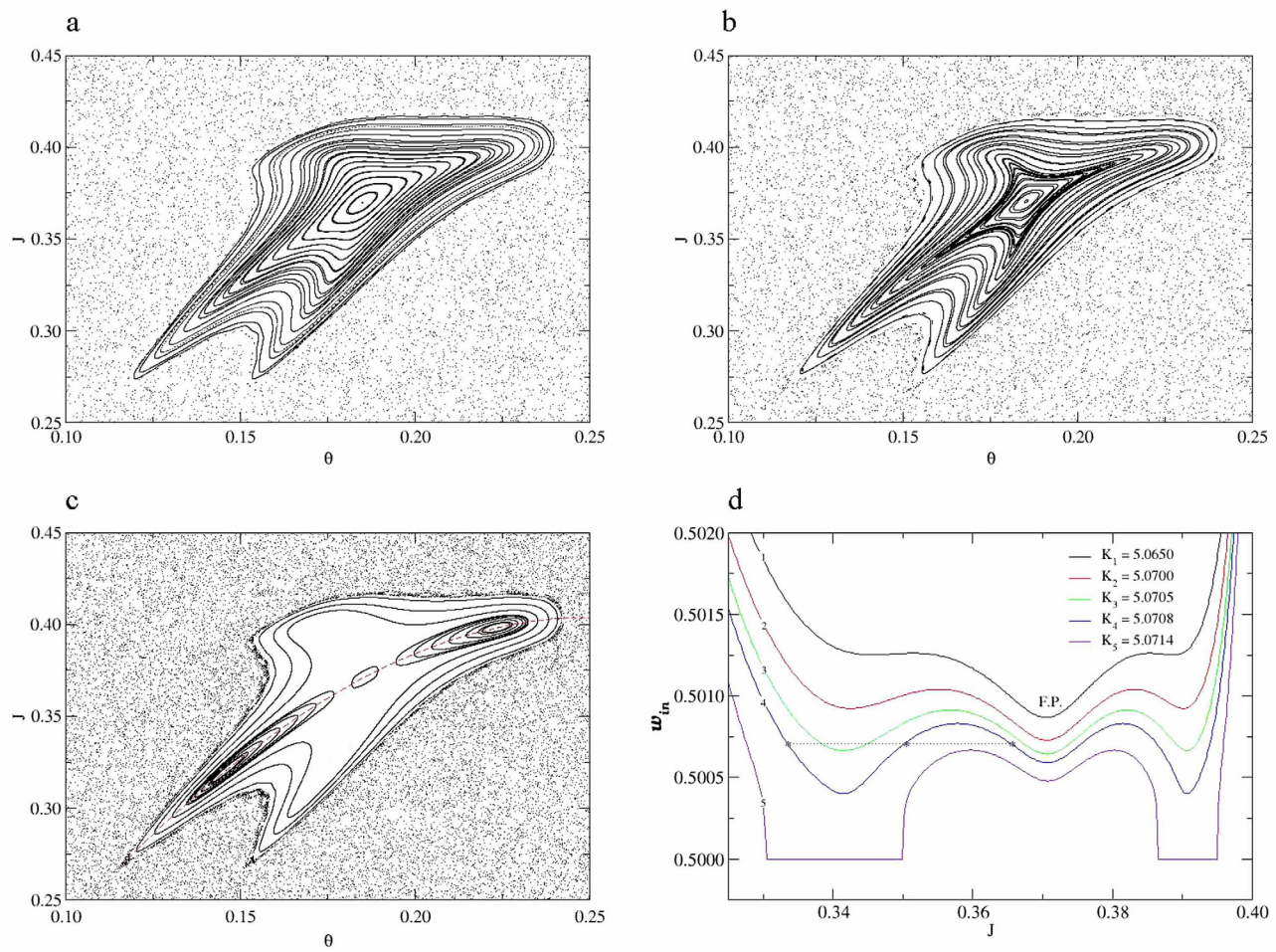

FIG. 6. The quadrupling bifurcation. (a) $K = 5.065$; (b) $K = 5.071$; (c) $K = 5.074$. (d) Five different internal rotation numbers. In the neighborhood of period-four orbit, there are two s-shearless tori. The dotted line in curve 4 indicates the same value of the rotation number for three different tori.

number profiles for $K = 5.0650$ to $K = 5.714$. To calculate these profiles, we choose a set of appropriate initial conditions disposed on the symmetry line $2J = -\frac{K}{2\pi}\sin(2\pi\theta)$ that crosses the two new elliptic points (the red dashed line in Fig. 6(d)). In the first profile at $K = 5.0650$, we observe the emergency of two bumps, one maximum and one minimum, corresponding to two secondary shearless tori. Consequently, as indicated in Fig. 6(b), the same rotation number may repeat up to three times. For $K = 5.0714$, the minimum bump reaches the value $\omega_{in} = \frac{1}{2}$ yielding two stable fixed points, so long as the maximum bump still exist and does not bifurcate for any lower order rational number.

This period-four bifurcation, which has not yet been predicted in the literature for twist maps, gives rise to two invariant shearless curves in contrast to the generation of one shearless curve in the tripling bifurcation. We would like to remark that the global presence of more than one shearless curve was studied in Ref. 15 to the standard nontwist map. The onset of two shearless lead to a nonstandard reconnection scenarios[15] that may differ, for example, to that shown in Fig. 5 of the present paper. Unfortunately, we were not able to verify the possible nonstandard scenarios near the quadrupling bifurcation because the two s-shearless tori cross high-order rationals in the rotation number profile (see Fig. 6(d)).

V. CONCLUSIONS

Until recently, the presence of a torus without twist had been credited only to nontwist maps. In the context of nontwist phase space, the torus without twist is called a shearless torus and can be verified as the maximum/minimum of the corresponding rotational number (Eq. (4)). Unexpectedly, it has been shown that a shearless torus can also emerge from secondary resonances of area-preserving twist maps in a neighborhood of the tripling bifurcation.[6] Theoretically, a shearless torus implies the local violation of important theorems that assume the nondegeneracy of the frequency; e.g., the KAM and Poincaré-Birkoff theorems. Furthermore, when periodic orbits collide with such a torus, we expect to observe a nontwist bifurcation in the reconnection process.

In the present paper, based on Ref. 6, we introduced the internal rotation number (Eq. (5)) as a numerical diagnostic to find the secondary shearless tori. With this procedure, we found bifurcation scenarios not only for the predicted tripling bifurcation but also for the quadrupling bifurcation first reported in this article. We investigated two systems: (1) the SNM and (2) the SM. We stress that all cases emphasized for the standard map were also found for the standard nontwist map. Although twist and nontwist standard maps have global differences in the phase space, they may have similarities

around the elliptic fixed point of stable islands, since we found s-shearless tori and reconnection processes in both maps. It is worth noting that our results have not been previously reported even though the standard map has been ostensibly studied. As the systems presented here represent a large number of Hamiltonian systems, it is possible to assume that the violation of the twist condition (Eq. (3)) and the emergence of nontwist phenomena near an elliptic fixed point may happen at least for one set-parameter family in the phase space of any system.

Comparing the examples presented here and in Ref. 6, we observe that in all cases the shearless torus appears when the remaining regular islands have reduced size and the perturbation parameter is high, therefore the systems gets further away from the integrable case and, eventually, the perturbed map may not be much useful to describe the dynamics of the considered system. Even so, several interesting properties have been reported for high values of the perturbing parameter. For example, the studies concerning the accelerator modes in standard twist map[28] and the rupture of the transport barrier in nontwist maps.[17,21] In our study, the described bifurcations appear isolated in phase space for some parameters. Consequently, higher parameter values do not guarantee any special concentration of secondary shearless tori. Thus, for high parameters between those of the tripling and quadrupling bifurcations, no other secondary shearless tori have been found. Moreover, we stress that our numerical procedure using the internal rotation number profile is definitive to find nontwist scenario around the elliptic fixed point for isolated bifurcation parameters.

Apart from the theoretical implications, we would like to discuss a possible application of the emergence of an s-shearless torus within the islands in SNM. There is numerical evidence[21] in the SNM that the breakdown of a tripling separatrix, at the edge of the chaotic sea, generates stickiness stronger than that generally observed. This effect modifies the transport in the shearless region even after the shearless torus has broken. We investigated the islands presented in Ref. 21 and we conclude that those islands of period-three, actually, originated from a tripling bifurcation of a s-shearless torus. The suggestion of the authors of the above paper is consistent and from the point of view of transport, this is interesting because it enhances the possibility of achieving a more efficient transport barrier. This strong stickiness of the broken period-three separatrix should be further explored, especially because the stickiness phenomenon has been shown to be of great importance in many branches of physics.

ACKNOWLEDGMENTS

The authors acknowledge the discussions and suggestions of Professor P. J. Morisson (The University of Texas at Austin). This work was partially supported by the Brazilian research agencies: CAPES, FAPESP, and CNPq.

[1]J. M. Greene, R. S. MacKay, F. Vivaldi, and M. J. Feigenbaum, Physica D **3**, 468 (1981).
[2]R. S. Mackay, J. D. Meiss, and I. C. Percival, Physica D **27**, 1–20 (1987).
[3]A. N. Lichtenberg and M. A. Lieberman, *Regular and Chaotic Dynamics*, 2nd ed. (Springer Verlag, Berlin, 1992).
[4]R. Balescu, Phys. Rev. E **58**(3), 3781 (1998).
[5]G. A. Oda and I. L. Caldas, Chaos, Solitons Fractals **5**, 15 (1995).
[6]H. R. Dullin, J. D. Meiss, and D. Sterling, Nonlinearity **13**, 203 (2000).
[7]H. R. Dullin and A. V. Ivarov, Physica D **211**, 47–56 (2005).
[8]D. Del-Castilho Negrete and P. J. Morrison, Phys. Fluids A **5**, 948 (1993).
[9]K. Ullmann and I. L. Caldas, Chaos, Solitons Fractals **11**, 2129–2140 (2000).
[10]P. J. Morrison, Phys. Plasmas **7**, 2279 (2000).
[11]M. Roberto, E. C. da Silva, I. L. Caldas, and R. Viana, Phys. Plasmas. **11**, 214 (2004).
[12]E. Petrisor, J. H. Misguich, and D. Constaniescu, Chaos, Solitons Fractals **18**, 1085 (2003).
[13]J. S. E. Portela, I. L. Caldas, R. L. Viana, and P. J. Morrison, Int. J. Bifurcation Chaos Appl. Sci. Eng. **17**, 1589–1598 (2007).
[14]J. Moser, Nach Akad. Weiss. Gottingen, Math. Phys. K1, IIa (1962).
[15]A. Wurm, A. Apte, K. Fuchss, and P. J. Morrison, Chaos **15**, 023108 (2005).
[16]A. Apte, A. Wurm, and P. J. Morrison, Chaos **13**, 421 (2003).
[17]D. del-Castilho Negrete, J. M. Greene, and P. J. Morrison, Physica D **91**, 1–23 (1996).
[18]J. E. Howard and S. M. Hohs, Phys. Rev. A **29**, 418 (1984).
[19]A. Wurm, A. Apte, and P. J. Morrison, Braz. J. Phys. **34**, 1700 (2004).
[20]K. Fuchss, A. Wurm, A. Apte, and P. J. Morrison, Chaos **16**, 033120 (2006).
[21]J. D. Szezech, Jr., I. L. Caldas, S. R. Lopes, R. L. Viana, and P. J. Morrison, Chaos **19**, 043108 (2009).
[22]E. G. Altmann, G. Cristadoro, and D. Pazó, Phy. Rev. E **73**, 056201 (2006).
[23]B. V. Chirikov, Phys. Rep. **52**, 263 (1979).
[24]J. D. Meiss, Rev. Mod. Phys. **64**(3), 795 (1992).
[25]S. Aubry, Physica D **7**, 240 (1983).
[26]T. Y. Petrowsky, Phys. Lett. A **117**(7), 328 (1986).
[27]G. Casati and B. V. Chirikov, *Quantum Chaos: Between Order and Disorder* (Cambridge University Press, Cambridge, 1995).
[28]Y. H. Ichikawa, T. Kamimura, T. Hatori, and S. Y. Kim, Prog. Theor. Phys. Suppl. **98**, 1–18 (1989).